Substituent Effects on Two-Dimensional Assembling and Chain Folding of Rigid-Rod Polymer Poly(*p*-phenyleneethynylene) Derivatives on the Solid/Liquid Interface

Sheng-Bin Lei,[†] Ke Deng,[†] Yan-Lian Yang,[†] Qing-Dao Zeng,[†] Chen Wang,*[,†] Zhun Ma,[‡] Pei Wang,[‡] Ying Zhou,[‡] Qu-Li Fan,[‡,§] and Wei Huang*[,‡,§]

National Center of Nanoscience and Technology, Beijing 100080, P. R. China, Institute of Advanced Materials, Fudan University, 220 Handan Road, Shanghai 200433, P. R. China, and Institute of Advanced Materials, Nanjing University of Posts and Telecommunications, Nanjing, 210003, P. R. China

Received December 13, 2006; Revised Manuscript Received March 24, 2007

ABSTRACT: The two-dimensional assembling behavior of a series of poly(*p*-phenyleneethynylene) (PPE) derivatives having identical conjugated backbone but different substituents and degrees of polymerization has been studied using scanning tunneling microscopy (STM). Submolecularly resolved STM images reveal diverse forms of chain folding in the assembled monolayer, allowing the analysis of the effects of polarity and concentration of substituents on the assembling behavior and chain folding of PPE. Theoretical simulations have been performed to understand the structural effects on the chain folding characteristics on the surface. The submolecularly resolved STM images also enable the quasi-quantitative determination of molecular weight and number-averaged degree of polymerization. The histograms of the contour length measured from the STM images agree well with the theoretical Schulz−Zimm distribution, indicating the potential capacity of the STM method for the estimation of molecular weight distribution of rigid-rod polymers.

Introduction

π-Conjugated polymers constitute the most important categories of materials used in the so-called "plastic electronics",[1] and they have been used in the fabrication of field-effect transistors (FETs), light emitting diodes (LEDs), and photovoltaic cells[2] and even "molecular wires" in molecular electronics.[3] Their physical properties depend not only on the intrinsic single molecular characteristics but also on the supramolecular organization of the films.[4] The film properties are determined by the nature of the molecular structures, functionalities, substrates, and film processing conditions.[5] Therefore, control of structural order on the molecular level in semiconducting materials, such as conjugated polymers has genuine importance to their electronic properties.[6]

Poly(*p*-phenyleneethynylene)s (PPEs)[7] are of particular interest because of their rigid-rod structure,[8] strongly anisotropic electronic properties, electroluminescence in blue-green region[9] and high and stable photoluminescence quantum yield.[10] These properties merit their promising potential applications for the development of liquid crystal-based photoluminescent display.[11] Their high and stable photoluminescence quantum yield are probably due to their rigid structure which limits potential nonradiative deactivation pathways.[12] PPEs have also been used as the emitting layers in LEDs.[13]

Studies on molecular packing,[14] energy migration,[15] polarized photoluminescence,[16] chromophore aggregation,[17] and charge carrier mobility[18] in phenylene ethynylene oligomers and polymers (PPEs) have been extensively pursued. While unsubstituted PPE is completely insoluble, the materials could be made soluble by attaching linear alkoxy side chains to the rigid-rod polymer backbone and by controlling their molecular weight.[19] Many reports on rigid-rod polymers show that a derivatization with long alkyl side chains not only enhances the solubility but also can lead to highly ordered supramolecular architectures in the solid state.[20] X-ray diffraction measurements on thin films of PPEs derivatized with linear or sterically hindered side chains show that polymers having identical conjugated backbone but different supramolecular structures in the solid-state could be achieved.[21]

On the basis of these findings, it can be presumed that the solid-state structures of derivatized PPEs could be controlled by the choice of side chains, and different supramolecular structures can be obtained with polymers having identical conjugated backbone. Because many electronic properties of conjugated polymers depend on the degree of order,[22] this structural concept can be an important tool to tailor the electronic properties of rigid-rod conjugated polymers. However, the current studies are solely carried out on bulk materials or films, the interface structures of these polymers which have direct relevance on the performance of devices is still unknown due to the limit of these conventional spectroscopic methods.

In comparison with atomic force microscopy (AFM), which is widely used for the investigation of mono- and multilayers of macromolecular systems,[23] STM enables researchers to image polymer chain conformations at the immediate interface of substrate with submolecular resolution.[24] Despite the wide application of STM in the investigation of surface assembling of single and multicomponent small organic molecules and model oligomers,[25−26] the application of STM in the investigation of interface structure of polymers is relatively limited. Nevertheless, the few available reports on regioregular poly(3-alkylthiophene)s (P3AT), poly[(*m*-phenylenevinylene)-*co*-(2,5-dioctoxy-*p*-phenylenevinylene)] (PmPV) and PPEs[24,27] have

* Corresponding authors. (C.W.) Telephone/Fax: +86-10-62562871. E-mail: wangch@nanoctr.cn. (W.H.) Telephone: +86-21-55664188. Fax: +86-21-65655123. E-mail: wei-huang@njupt.edu.cn.
[†] National Center of Nanoscience and Technology.
[‡] Institute of Advanced Materials, Fudan University.
[§] Institute of Advanced Materials, Nanjing University of Posts and Telecommunications.

10.1021/ma062855n CCC: $37.00
Published on Web 05/26/2007

Scheme 1. Molecular Structures and GPC Analysis of the PPE Polymers[a]

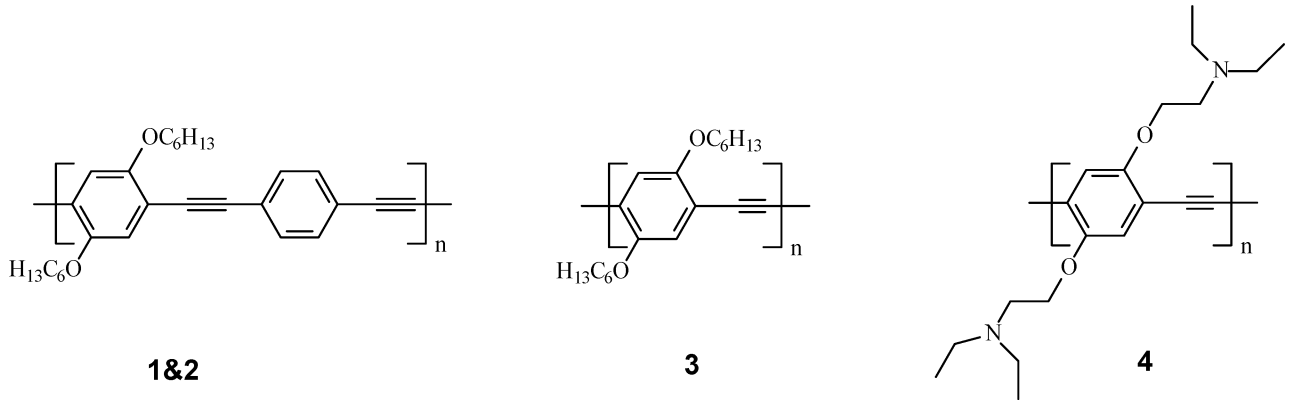

[a] Key: (1) $M_n = 3500$, $M_w = 6200$, DI = 1.78; (2) $M_n = 7300$, $M_w = 12100$, DI = 1.66; (3) $M_n = 9700$, $M_w = 22000$, DI = 2.27; (4) $M_n = 18900$, $M_w = 38600$, DI = 2.04

undoubtedly shown the ability of STM to reveal chain folding and to determine polymer weight. *However, the effects of molecular structures, such as regioregularity of the backbone, structure, and polarity of substitutents, on the microscopic assembling behavior of the conjugated polymers on the interface are yet to be fully clarified. In this work, the assembling behavior of a series of PPEs with identical conjugated backbone but different side chains was studied.* The side chain structure caused different packing of these compounds on the interface has been directly visualized with submolecular resolution. The STM results demonstrate that the concentration and structure of side chains not only affect the supramolecular order on the interface but also affect the chain folding characteristics in the adsorbed layer. The degrees of polymerization of these polymers are directly determined by STM and compared with that obtained from conventional gel permeation chromatography (GPC) measurements. The statistics of the polymer contour length from the submolecularly resolved STM images shows satisfactory agreements with the theoretically expected Schulz−Zimm distribution, demonstrating the reliability of STM methods.

Experimental Section

Materials. All manipulations involving air-sensitive reagents were performed under an atmosphere of dry argon. All reagents, unless otherwise specified, were obtained from Aldrich Chemical Co. and used as received. All the solvents used were further purified before use.

Polymerization. The precursors for polymerization are synthesized according to the literature (some details could also be found in the Supporting Information).[28] Sonogashira polycondensations were conducted in the presence of 4% Pd $(PPh_3)_4$ and 4% CuI in the solution of diisopropylamine/toluene (1:2) at 60 °C for 24 h and then subjected to a $CHCl_3/H_2O$ workup. The combined organic phase was washed with NH_4OH (50%) twice, water twice, and brine and then dried over $MgSO_4$. The solvent was removed in vacuum, and the residue was redissolved in a minimum of $CHCl_3$ and the solution was reprecipitated in methanol twice. The mixture was filtered, and dried under vacuum at room temperature. For polymer **1**, in order to control the molecular weight, 10% iodobenzene was added as end-caps. P1 and P2: 0.52 g (yield 78%) for P1 and 0.46 g (yield 81%) for P2, respectively. ^{1}H NMR ($CDCl_3$, ppm): δ 7.54 (d, 2H), 7.34 (d, 2H), 7.02−7.00 (m, 2H), 4.03 (m, 4H), 1.85 (br, 4H), 1.52 (br, 4H), 1.36 (br, 8H), 0.89 (m, 6H). ^{13}C NMR ($CDCl_3$, ppm): δ 153.68, 133.60, 128.20, 117.00, 114.81, 94.97, 84.97, 70.90, 31.85, 29.55, 25.97, 22.88, 14.30. P3: 0.61 g (yield 76%). ^{1}H NMR ($CDCl_3$, ppm): δ 7.02−6.96 (m, 2H), 4.03 (m, 4H), 1.86 (br, 4H), 1.52 (br, 4H), 1.37 (br, 8H), 0.91 (m, 6H). ^{13}C NMR ($CDCl_3$, ppm): δ 154.60, 117.92, 115.03, 101.62, 70.12, 32.01, 29.70, 26.07, 23.02, 14.41. P4: 0.42 g (yield 85%). ^{1}H NMR ($CDCl_3$, ppm): δ 7.04 (s, 2H), 4.12 (t, 4H), 2.95 (t, 4H), 2.70 (q, 8H), 1.08 (t, 12H). ^{13}C NMR ($CDCl_3$, ppm): δ 153.8, 117.5, 114.6, 91.9, 68.8, 52.1, 48.4, 12.6.

GPC Measurements. The GPC measurements were performed on a Shimadzu LC10A chromatograph equipped with Shim-pack GPC-803, 804, and 8025 columns and refractive index detector, using seven kinds of polystyrenes (MW from 1000 to 240 000 Da) as external standards and THF as an eluent at a flow rate of 1.0 mL/min and 35 °C. The sample solution concentrations are around 10 mg/mL, and 20 μL solutions were injected for each example.

STM Characterization. The polymers are dissolved in toluene with a concentration of about 1 mg/mL. Assembling thin film of these polymers are formed by casting a drop of the toluene solution (1 μL) on a freshly cleaved highly oriented pyrolytic graphite (HOPG). The STM characterization of the assembling film was carried out with a Nanoscope IIIa (Veeco Metrology) on a liquid/solid interface. The liquid/solid interface was formed by adding 1 to 2 μL of 1-phenyloctane between the STM tip and the sample surface. Though STM characterization could also be carried out at the dry sample surface, our experience demonstrates the formation of a liquid/solid interface can improve the image quality. 1-phenyloctane could also be used as solvent, but the solubility of PPEs in this solvent is lower and sometime molecular fractionation may occur (see Supporting Information). The statistic of the contour length of polymer chains was measured manually from different images obtained on different sites of different samples to ensure the reliability. The theoretical Schulz−Zimm distribution curve was computed according to Schulz−Zimm function using the number-averaged degree of polymerization obtained from STM.

Computational Details. We performed theoretical calculation using density functional theory (DFT) provided by the DMol3 code.[29] The Perdew and Wang parametrization[30] of the local exchange-correlation energy are applied in the local spin density approximation (LSDA) to describe exchange and correlation. We expand the all-electron spin-unrestricted Kohn−Sham wave functions in a local atomic orbital basis. In such double-numerical basis set polarization is described. All calculations are all-electron ones, and performed with the extrafine mesh. Self-consistent field procedure is done with a convergence criterion of 5−10 au on the energy and electron density.

Results and Discussion

1. Surface Assembling of PPE Bearing Different Side Chains. Scheme 1 shows the molecular structures of the compounds investigated in this work. Polymers **1** and **2** possess identical structure but different degree of polymerization. Polymers **3** and **4** bear the same conjugated backbone with polymers **1** and **2**, but the concentration of side chains is twice of that of polymers **1** and **2**. The difference between **3** and **4** is

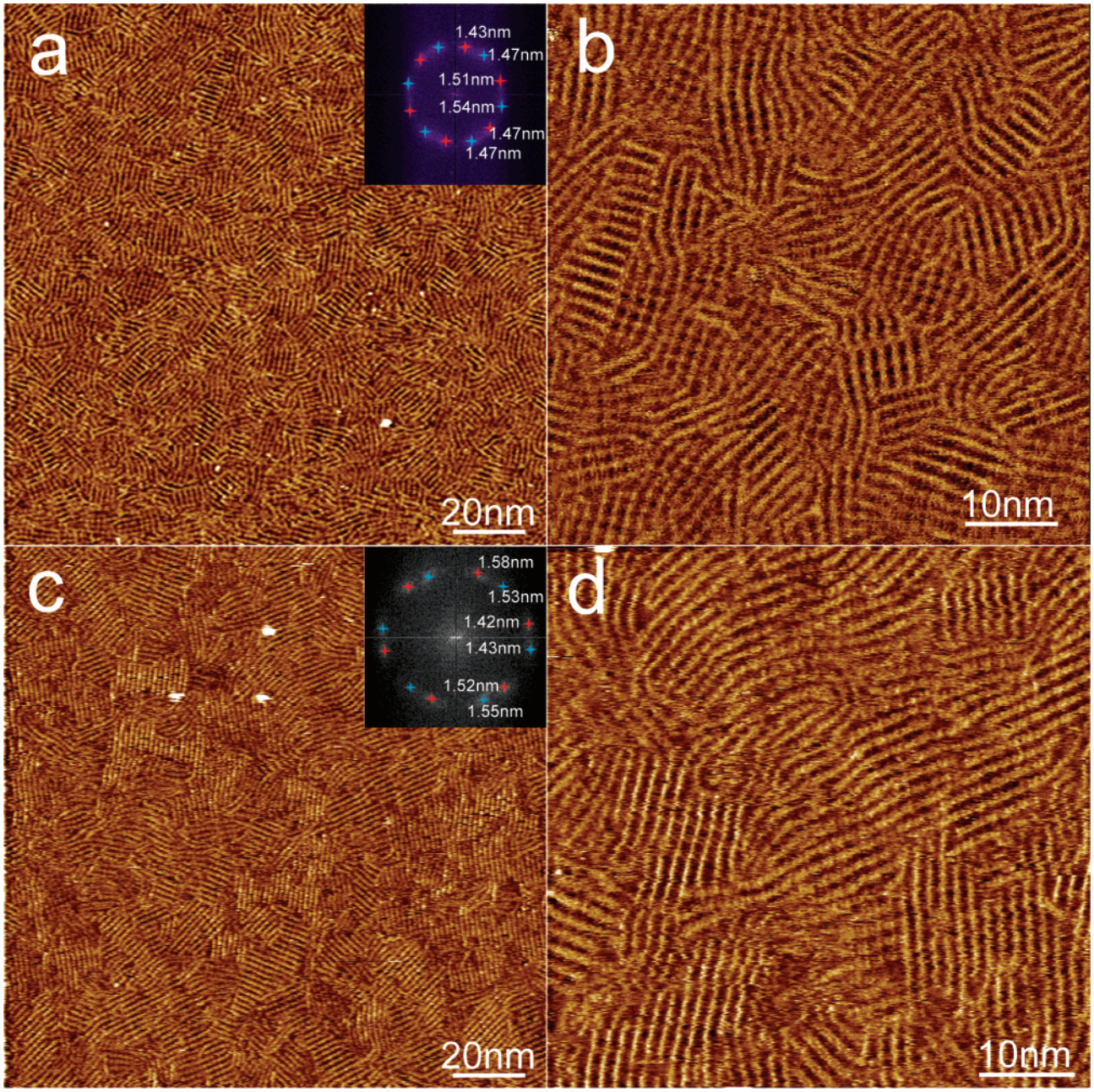

Figure 1. STM images obtained on the assembling structure of polymers **1** and **2**. Imaging conditions: (a and b) 950 mV, 600 pA; (c and d) −820 mV and 540 pA. Inserted in parts a and c is the FFT of the corresponding image from which the interchain distance could be estimated.

the structure of the side chains, where the side chains of polymer **4** have an amino group which makes it more hydrophilic in comparison with the hexyloxy group. In addition the branched structure brings greater steric hindrance between the side chains. Powder diffraction and electron microscopy studies on the solid-state structure of PPEs reveal either lamellar or interdigitated phase depending on the concentration of solubilizing side chains per repeating unit.[31] In this study, we utilize STM and other techniques to investigate the effects of side chain structures and concentration, degree of polymerization, etc. on the assembling and chain folding characteristics of the PPE compounds on the interface.

1.1. Influence of Degree of Polymerization. Figure 1 shows the large scale and high-resolution STM images of the assembling structure of polymers **1** and **2**. Benefiting from the strong interaction between the high hydrophobic hexyloxy side chains with the graphite substrate, polymers **1** and **2** adsorb stably on the surface of graphite and form a close packed monolayer. In these monolayers both the conjugated backbone and the side chains lie flat on the basal plane of HOPG. The conjugated backbone appears with higher contrast due to higher tunneling probability associated with the π electrons.[27] The interchain distance in both the monolayer of polymers **1** and **2** are estimated to be about 1.5 nm, in good agreement with that expected from the conformation that the hexyloxy side chains are fully extended and interdigitated with that from the neighboring molecule (Figure 2b). Normally the interdigitation of the side chains will increase interactions between adjacent polymer chains and gives extra stability to the assembling monolayer.[24,27] The polymer concentration used in the current study results in nearly full coverage of these compounds. According to our observation these two polymers form perfect monolayers on graphite in the view area of STM. Because of the identified structure of these two compounds the assembling structures are also nearly identical except the longer contour length of polymer **2**. Another observation is that in the

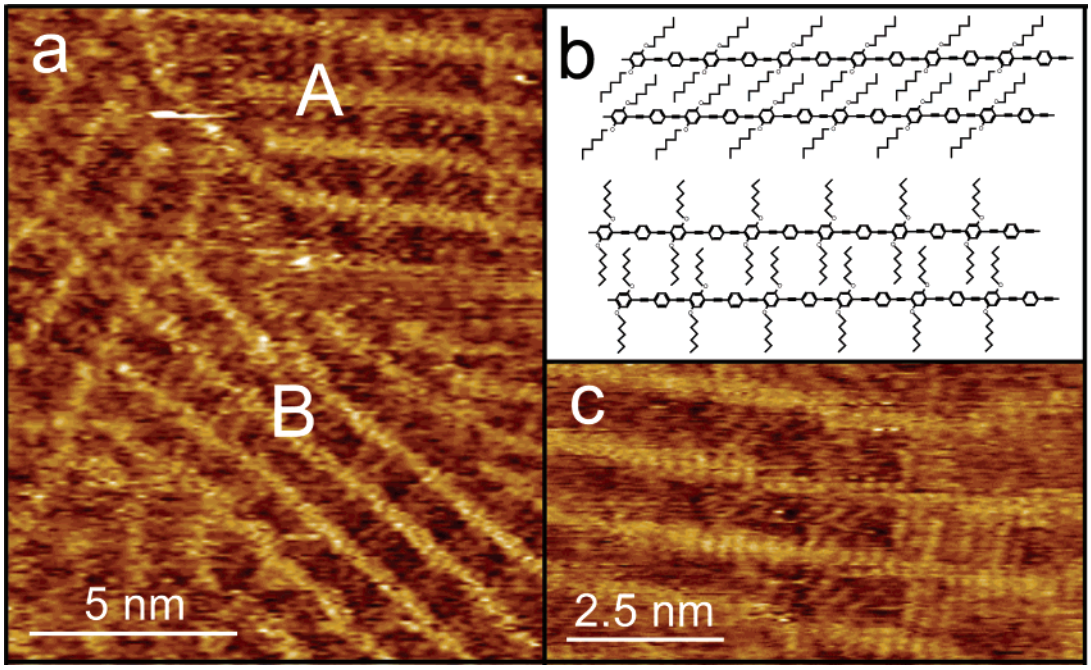

Figure 2. High-resolution STM images obtained on the assembly of polymer **1**. Different orientation of the side chains could be clearly observed in the area marked A and B. Part b shows the schematic model for the different packing of the side chains. In some cases the different orientation of the side chains could even be seen along the same polymer backbone as shown in part c. The images were obtained under bias 950 mV with a set point of 600 pA.

monolayer of **1**, some small domains formed by several parallel oligomers are occasionally observed due to the small degree of polymerization.

It is not surprising that the molecular chains of these compounds align along preferred directions according to the 3-fold symmetry of the HOPG substrate due to the expectable $\pi-\pi$ interaction of the conjugated backbone with the substrate and the registered adsorption of aliphatic side chains.[26b] However, one surprising observation is that two sets of 3-fold symmetrical points can be identified in the fast Fourier transformation (FFT) of the STM images (Figure 1, parts a and c), indicative of two different orientations of the polymer chains in the monolayer with respect to the substrate. FFT of the STM images obtained from the assembling monolayer of these two compounds all show this phenomenon, excluded the possibility of tip artifacts and substrate defects. These two sets of points are rotated for about 30° from each other. Both of these two sets of points correspond to a repeating periodicity (reflecting the interchain distance in the ordered domain of the monolayer) ranging from 1.42 to 1.55 nm.

Considering the rotation of the C(phenyl)−O bonds connecting the hexyloxy side chains with the conjugated backbone, two different orientations of the side chains with respect to the backbone can be expected, as shown in Figure 2b. The side chains orientated in a direction about 60° from the backbone axis in the "tilt" conformation (shown in the upper part of Figure 2b), while nearly perpendicular to the backbone in the "perpendicular" conformation (Figure 2b, lower part). Because of the registered adsorption of the aliphatic side chains, this difference in side chain orientation will result in different orientation of the polymer chains with respect to the substrate lattice. Though the different orientation of the side chains will slightly change the interchain distance in the ordered domains (1.45 vs 1.53 nm), it is difficult to distinguish this difference by STM due to possible thermal drifts during scanning. However, the stable adsorption of these compounds allows us to image the assembled monolayer in a nearly atomic resolution, and in high-resolution images different orientations of the aliphatic side chains can be clearly distinguished (Figure 2a). In the domains marked A and B the orientation of the side chains are in excellent accordance with the proposed model in Figure 2b. In some areas, these two orientations can be observed to coexist in the side chains of a same polymer molecule (Figure 2c).

1.2. Influence of the Concentration of Side Chains. Parts a and b of Figure 3 show the assembling structure of polymer **3** on a graphite surface. In comparison with polymer **2** whose degree of polymerization is very similar (see Table 1), two observations should be noticed. First is the relatively low order of assembling monolayer where many vacancies or defects can be found. The second is that the polymer chains seem more flexible and chain folding are more frequently observed in the monolayer. Many hairpin foldings could be revealed and the theoretically "rigid" backbone rarely persists straight features on the surface. FFT of the STM image show expected 3-fold symmetry. Different from that of polymers **1** and **2**, only one set of points are observed. The interchain distance in the assembling monolayer is estimated to be 1.64 nm, in good agreement with the previous observation by Rabe et al.[27] Due to the small distance between the neighboring side chains (0.69 nm) interdigitation is impossible, the 1.64 nm interchain distance is also smaller than the 1.8 to 1.9 nm distance expected from a hexyloxy side chain fully extended lamellae conformation. This may indicates that the side chains are not well-ordered in the monolayer, and the alignment of the polymer is only determined by the interaction between the backbone and the substrate. This proposition well explains that only one set of 3-fold symmetry points in the FFT of STM image are identified. And the disordered side chain hypothesis also agrees with the low order packing and high flexibility of polymer chains observed by STM.

The 2D assembly structures of polymer **3** with high side chain concentration and polymers **1** and **2** with low side chain concentration agree well with the solid-state structure of lamellae

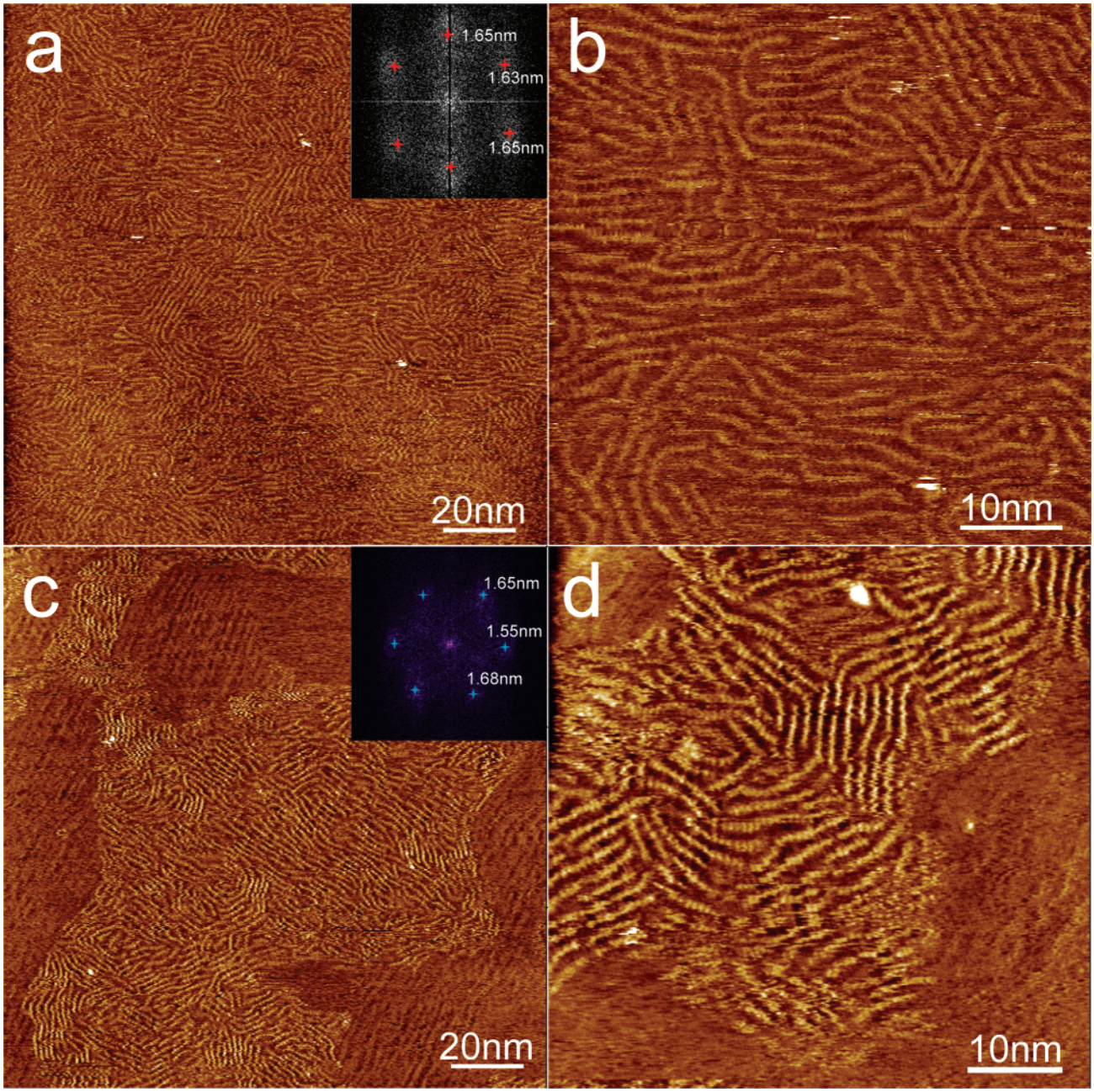

Figure 3. Assembling structure of polymer **3** (a and b) and polymer **4** (c and d). Both these polymers form lamellae phase on the interface and polymer **3** shows higher flexibility and forms diverse forms of chain folding. Imaging conditions: (a and b) 890 mV, 340 pA; (c and d) 760 mV, 590 pA.

Table 1. Comparison of the Molecule Weight and Degree of Polymerization of the PPEs Determined via STM and GPC

compound	av contour length (nm)	mol wt (from STM)	no.-av mol wt (from GPC) (Da)	deg of polymerization STM/GPC[a]
PPE1#	8.6	2500	3500	6.2/8.7 (0.71)
PPE2#	14.8	4300	7300	10.7/18.2 (0.59)
PPE3#	14.8	6400	9700	21.4/32.3 (0.66)
PPE4#	9.5	4400	18 900	13.8/57.2 (0.24)

[a] The number in parentheses indicates the ratio of degree of polymerization determined from these two methods.

and interdigitated phase, respectively.[28] For the lamellae phase formed by polymer **3**, the interaction between neighboring polymer chains are expected to be relatively weak in comparison with that in the interdigitated phase, this decrease in interaction between polymer chains may afford for the lower order in the assembling monolayer and higher flexibility of the polymer chains. Investigations on solid-state structures of PPEs show that when long alkyl or alkoxy groups are present on the rigid backbone, the polymer structure is almost dominated by side chain packing.[28] Our present observations demonstrate that this is also the case for the interface structure.

1.3. Influence of the Side Chain Structure. The assembling structure of polymer **4** is shown in Figure 3, parts c and d. In comparison with the other three polymers bearing hexyloxy side chains, the side chains of polymer **4** have amino group which introduce higher polarity and hydrophilicity to the polymer, the branched structure also increases the steric hindrance between these side chains, inhibiting their interdigitation in the assembling monolayer. When adsorbed on the highly hydrophobic graphite surface, the high polarity of the side chains significantly decreases the affinity of the polymer to the graphite surface. This has been confirmed by the lower coverage in STM images. STM observations also indicate the stability of the adsorbed

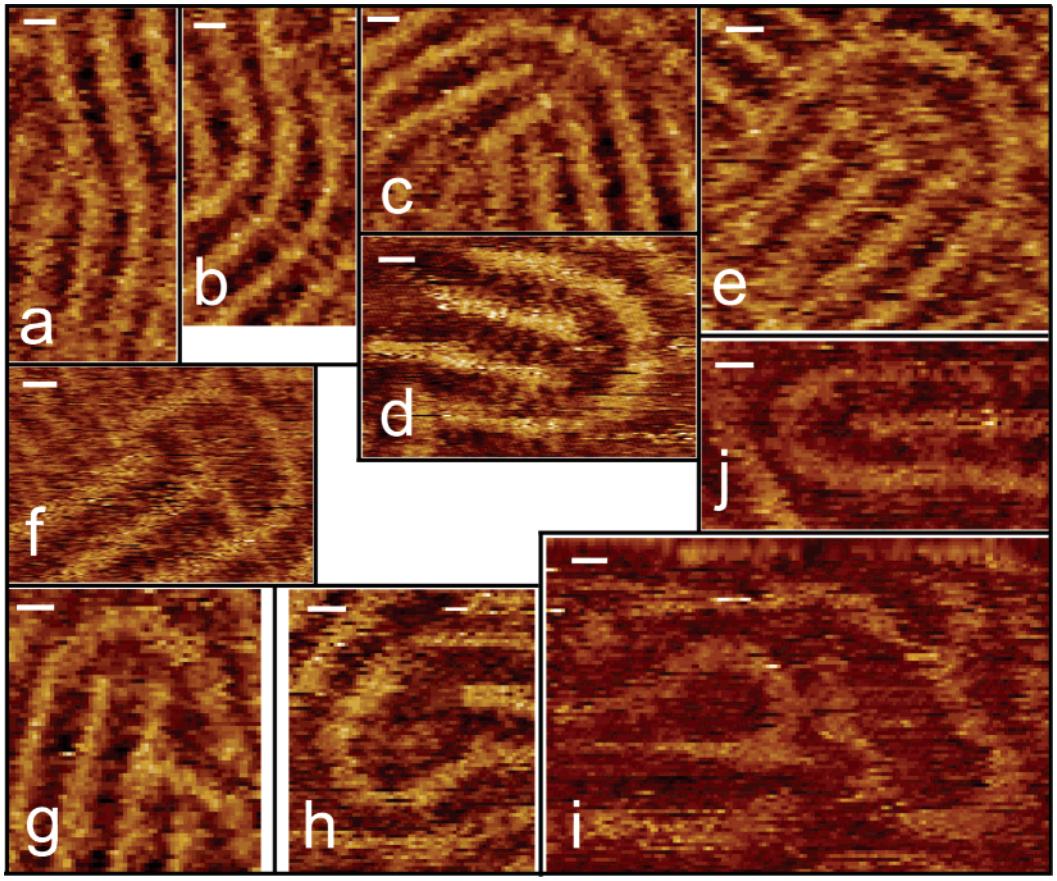

Figure 4. Different types of chain folding observed in the assembling structure of the PPEs on the interface. Though the lager scale foldings could be found in the assembly of all these polymers, the chain folding with a diameter of 3.2 nm (h, i, and j) could only be observed in the assembly of polymer **3**. The scale bar in the images corresponds to 1 nm.

monolayer is lower in comparison with the other three polymers and can be easily destroyed by the scan of STM tip. However, by carefully adjusting the imaging conditions submolecularly resolved images could be obtained on polymer **4**. As shown in the inset of Figure 3c, the FFT of the STM image also shows 3-fold symmetry, the same as that of polymer **3** in which only one set of points present. The interchain distance is estimated to be 1.63 nm. Because of steric hindrance of the ethyl groups, interdigitation of the side groups is impossible for polymer **4**. The side chains may align disordered in the monolayer, the same as that observed in the assembly structure of polymer **3**.

Comparing the assembling behavior of polymers **3** and **4**, the effect caused by the structure of side chains is the different affinity to the substrate. The higher polarity of amino groups significantly reduces the affinity of polymer **4** to the hydrophobic graphite surface, changing full coverage monolayer of polymer **3** into isolated domain structures of polymer **4**. Regarding the alignment of side chains, both the side chains of these two polymers are disordered in the monolayer. Unlike the interdigitated side chains of polymers **1** and **2**, no details can be revealed by STM on the alignment of side chains for polymers **3** and **4**.

In brief, the difference in degree of polymerization between polymers **1** and **2** whose structure is identical does not show significant differences in assembling behavior except for the size of ordered domains. In contrast, the increase in side chain concentration causes significant differences not only in assembling behavior but also in the forms of chain folding (will be discussed below). The steric hindrance prevents the interdigitation of side chains and makes the polymer chains more flexible and mobile in the monolayer. Though the number of side chains is the same for polymers **3** and **4**, the higher polarity of amino group greatly reduces the affinity of polymer **4** to the highly hydrophobic graphite surface, make the adsorption less stable.

2. Chain Folding in the Assembling Monolayer. PPE, made of alternating phenyl and ethynyl groups along the main chain, belongs to the rigid-rod type of polymers that are expected to possess a conjugated backbone with a linear conformation. However, STM observations here and by other groups previously[27] demonstrate that the behavior of this type of molecules is well described as elastic rods. For the fraction of long molecules, bending are normally observed in the assembling monolayer which is not surprising as the expected finite persistent length.[27,28] Due to the high stability of the assembling structures, diverse chain foldings could be observed by STM with submolecular resolution in the monolayer of these compounds, allowing the investigation of impacts of side chains on the chain conformation of such rigid polymers. Another interesting point is to compare the chain folding behavior of this rigid-rod polymer with that of the more flexible poly(3-alkylthiophene)s (P3AT).[24] This will help us to understand the controlling factors of the polymer chain folding on the interface. Bending of the conjugated backbone from 0 to 180° all could be found in the monolayer of these PPEs. Though bending of a specific angle (such as 120°) in a long range is not surprising if we consider the PPE polymer chains as an elastic rod, hairpin folding within only a few repeating units is indeed surprising for such a rigid-rod polymer. All the typical forms of chain folding observed in the assembling monolayer of these polymers are shown in Figure 4.

Though most of these forms of chain folding could be observed in the assembling monolayer of all these PPEs,

indicating chain folding is a common phenomenon of these rigid-rod polymers on the interface, chain folding Figure 4, parts h, i, and j, could only be observed in the monolayer of polymer **3**. These hairpin foldings all possess the smallest diameter of about 3.2 nm, this means the polymer chains bend for 180° in a length scale of about seven to eight repeating units. For comparison, poly(3-hexylthiophene) (P3HT) form hairpin folding in a length scale of seven repeating units (with a diameter of 1.4 nm) and PmPV in a length scale of three repeating units (with diameter of 2.9 nm). Both of these two polymers form chain foldings with a cis conformation.[24] The torsion of the bond angles of the backbone is less than 1% for these polymers. In contrast to the rigid-rod polymer PPE, the chain folding can only be realized by bond torsion in the conjugated backbone. The realization of a hairpin folding in a length scale of seven repeating units requires bond torsion of about 5% of the bond angle. In comparison with P3HT where the realization of chain folding does not result in significant energy rise, the large bond torsion in the hairpin folding of PPEs is expected to cause significant rise of the system energy.

To further understand the different chain folding behavior of the low and high side chain concentrated PPEs, we performed theoretical calculation using density functional theory (DFT). Two aspects were mainly considered: the folding of the backbone and interchain interaction. For the first aspect, we examined the effect of the folding of backbone on the system energy. Three conditions are considered for the same hairpin folding with 3.2 nm diameter: pure PPE without side chains and PPE with low and high concentration of hexyloxy side chains according to the structure of polymers **1** and **3**. In comparison with the linear rigid-rod conformation, in the hairpin conformation the system energy is 18.75, 14.68, and 16.29 kcal/mol higher for pure PPE without side chains and polymers **1** and **3**, respectively. This means that for single polymers **1** and **3**, the energy difference is mainly caused by folding of the backbone and the stability of the same folding of polymer **1** is slightly more stable than that of polymer **3**.

However, this contradicts with the experimental result, since our STM observations indicate only polymer **3** could achieve hairpin folding with diameter 3.2 nm, while polymer **1** could only fold with larger scale. Thus, another possible factor, the interchain interaction in the assembly, is considered. Our simulation demonstrates the interchain interaction is 5.846 and 3.047 kcal/mol per repeating unit for polymers **1** and **3**, respectively (note that the length of repeating unit of polymer **1** is two times of that of polymer **3**). This means the interchain interaction between polymer **3** is about 5% stronger than that of polymer **1** for a polymer chain with the same length (for example, for a polymer chain with the length of 11 nm, the interaction energy is calculated to be 46.77 and 48.75 kcal/mol, respectively, for polymers **1** and **3**). This is quiet surprising since we always expect a stronger interchain interaction in the interdigitated conformation. We attribute this to the short length of the hexyloxy chain in which the increase in interaction for an interdigitation conformation is not significant.

The simulation results demonstrate both the energy rise caused by the backbone folding and the interchain interaction indicate polymer **1** with low side chain concentration should more easily form hairpin foldings with the smallest diameter, though the energy difference is not so significant for these two polymers. This is clearly conflict with the STM observations. This means there should be other factors effecting the polymer chain folding. *Here we suggest that a geometrical effect should be responsible for such a folding discrepancy*. For the interdigitated phase in polymer **1**, the alkane branches of adjacent polymers interlock with each other, while in the lamellae phase of polymer **3**, the alkane branches of polymer just tail-to-tail interact with that from the adjacent polymer chain. Thus, the adjacent polymer chains in the lamellae phase could slide with respect to each other along the chain axis without causing apparent increase of system energy, while this is impossible in the interdigitated phase. It is possible that the interlocking alkane branches between two polymer **1** molecules puts more restriction on the polymer chains and prevents the short-diameter folding. In other words, the interlocking between polymer chains in the interdigitated phase makes the polymer molecules act in a collective manner and helps the polymer chain to persist "rigid". This is consistent with the observation that conjugated backbone of polymers **1** and **2** can readily persist linear in the assembling layer in comparison with polymer **3**.

It is also interesting to compare the chain foldings of these rigid PPEs with that of the more flexible P3ATs. Our observations here illustrate the PPEs form nearly all possible foldings with the angle ranging from 0 to 180°. While for P3ATs, only particular angle 0, 60, and 120° foldings were observed (see Supporting Information, Figure S4). This means for the flexible P3ATs, the molecular folding of the polymer chain is dominated by the epitaxial effect of the side alkyl chains. However, for PPEs, the rigidity of the backbone plays an important role in the molecular folding on the surface. It is noticeable that hairpin foldings is the most common folding characteristics for P3ATs which means it does not cause significant energy rise in compare with the linear conformation. While for the rigid PPEs, slight bending in a large scale is prevalent. For understanding of this aspect, further theoretical simulation is undergoing.

3. Direct Determination of Molecular Weight and Distribution of Polymerization. The submolecular resolution obtained on these polymers allows the identification of the chain ends, thus making it possible to quasi-quantitatively determine the contour length of the individual macromolecules with high accuracy (a few angstroms). Figure 5 shows the distribution of the contour length of polymer **1** to polymer **4**, each obtained by statistical analysis of the contour length of more than 1000 molecules estimated from different images obtained from different areas of the sample. From these histograms several important parameters of these polymers, such as the degree of polymerization, the average molecular weight, and the molecular weight distribution, could be determined.

The average molecular weight and degree of polymerization estimated from the STM results and GPC have been shown in Table 1. It can be seen that the molecular weight and degree of polymerization estimated from STM is apparently smaller than those obtained by GPC. For polymers **1**−**3**, the molecular weight and degree of polymerization is about 60−70% of that measured by GPC. For the rigid-rod polymers, such as PPEs, GPC vs polystyrene (PS) overestimates molecular weight. The groups of Tour and Müllen have investigated this point either by using defined oligomers or comparing GPC results with end group analysis by ^{1}H NMR, and find out GPC vs PS overestimate the molecular weight of PPEs by a factor of 2−3.[32] Thus, our STM measurements show reasonable consistence with their results. Our current results also indicate the GPC method shows dependence on molecular weight and side chain properties of the polymers. It overestimates molecular weight for a larger extent for larger polymers and polymers with polarizable side chains. This is because GPC method is sensitive to aggregation of polymer chains which is a normal phenomenon of conjugated rigid-rod polymers.

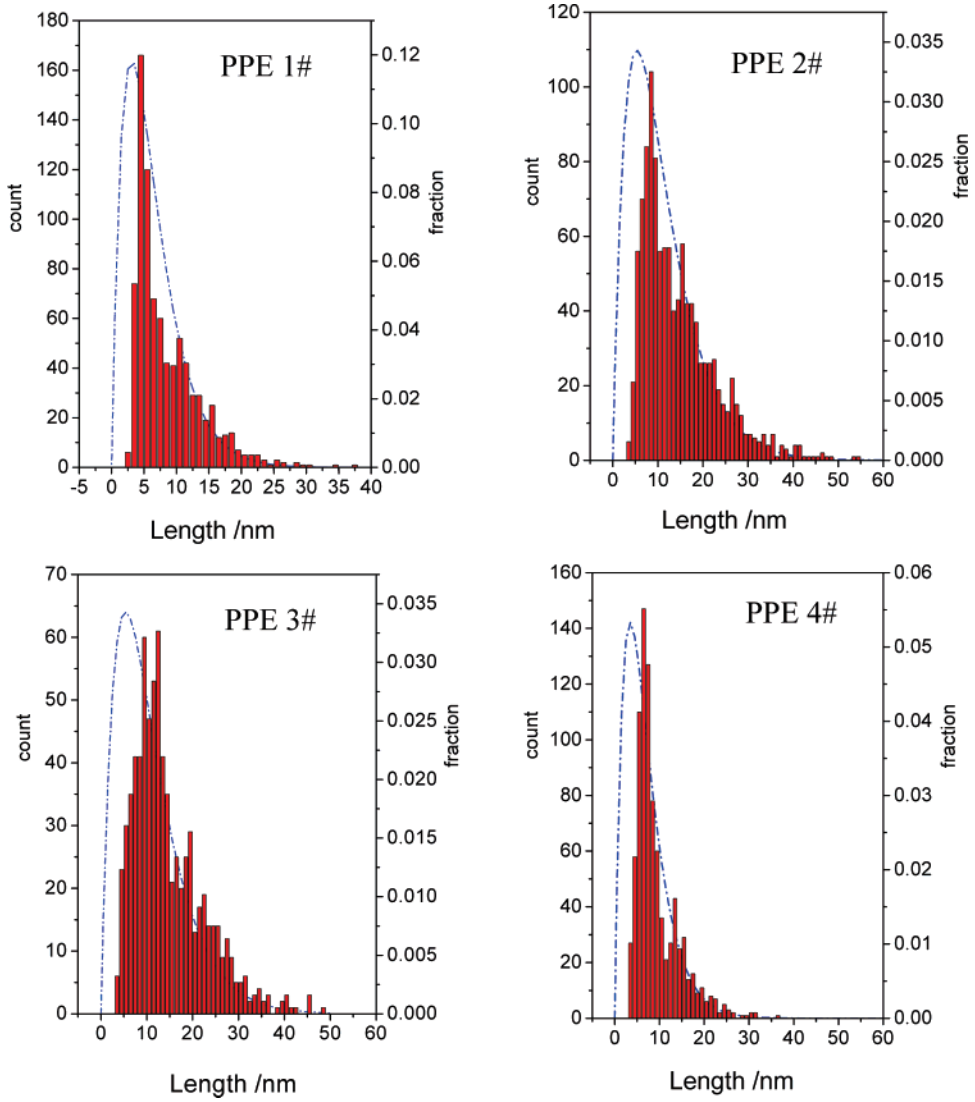

Figure 5. Histogram shows the statistic of the contour length of the polymer chains in the assembling layer on the interface. The dotted line represents the Shulz−Zimm fit of the molecular weight distribution.

The molecular weight distribution of polymers obtained from the polycondensation reaction could be theoretically described by the Schulz−Zimm distribution. The mole fraction distribution of compounds **1**−**4** could be computed according to Schulz−Zimm function using the number-averaged degree of polymerization obtained from STM. These distributions are plotted in Figure 5 as dot-dashed lines. A good agreement between the histogram and the Schulz−Zimm curve could be clearly seen, indicating STM could provide a reasonable evaluation of the molecular weight distribution of the rigid rod polymer. It is worth noting that in our case no discernible molecular weight fractionation has been observed, which had been reported by Rabe et al. previously.[27] One possible factor is that we use the number-averaged degree of polymerization obtained from STM while in their report this parameter is obtained from ^{1}H NMR analysis of end groups. Another possibility is the different procedure for the sample preparation. In our procedure toluene is a more favorable solvent for the polymers and the concentration is also lower, so that aggregation of larger polymers in the solution could be reduced. The solvent effect may also accounts for the remarkably huge difference between molecular weight estimated by STM and GPC for polymer **4**. The polar side chains of this polymer may induce aggregation of the molecules in the nonpolar toluene and 1-phenyloctane solvents, which prevents the adsorption of larger polymers. Thus, the possible solvent effect on the conformation and fractionation of the polymer chain on the surface remains to be an interesting topic and will be addressed in our future work.

In comparison with GPC method, the advantage of the STM method is that it could determine the averaged molecular weight and degree of polymerization independent of the standard sample, therefore possibly lead to improved reliability of the measurements of the averaged molecular weight and degree of polymerization.

Conclusion

STM investigations on the PPEs with different substituent side chains and polymerization demonstrate that the assembling and polymer chain folding characteristics of such rigid-rod polymers on the interface is dominated by the interaction between the side chains. Comparison of the chain folding of these rigid-rod polymers with that of the more flexible P3ATs illustrates besides the interaction between polymer chains or the interaction between the side chains the rigidity of the conjugated backbone also plays an important role on the molecular assembling and chain folding on the interface. The submolecular resolution STM images also enable us to quasi-quantitatively determine the degree of polymerization and

molecular weight distribution of these polymers. Comparison of the results obtained from STM with that from GPC enables us to understand how the structural factors such as degree of polymerization, concentration, and structure of side chains influence the measurement of GPC. The current results not only proved STM as a useful tool for the investigation of conjugated polymers but also will contribute to the understanding of the behavior of these polymers on the interface.

Acknowledgment. The authors are grateful for the financial support from the National Natural Science Foundation (Grant No. 50573089).

Supporting Information Available: Text giving experimental and computational details of the theoretical modeling, a scheme showing synthetic route for monomers and polymers, and figures showing simulated molecular models and some high-resolution STM images. This material is available free of charge via the Internet at http://pubs.acs.org.

References and Notes

(1) Moore, S. K. *IEEE Spectr.* **2002**, *39*, 55.
(2) (a) Yu, G.; Gao, J.; Hummelen, J. C.; Wudl, F.; Heeger, A. J. *Science* **1995**, *270*, 1789. (b) Bourroughes, J. H.; Bradley, D. D. C.; Brown, A. R.; Marks, R. N.; MacKay, K.; Friend, R. H.; Burn, P. L.; Holmes, A. B. *Nature (London)* **1990**, *347*, 539. (c) Sirringhaus, H.; Tessler, N.; Friend, R. H. *Science* **1998**, *280*, 1741.
(3) (a) Bumm, L. A.; Arnold, J. J.; Cygan, M. T.; Dunbar, T. D.; Burgin, T. P.; Jones, L.; Allara, D. L.; Tour, J. M.; Weiss, P. S. *Science* **1996**, *271*, 1705. (b) Lindsey, J. S. *New J. Chem.* **1991**, *15*, 153. (c) Mirkin, C. A.; Ratner, M. A. *Annu. Rev. Phys. Chem.* **1992**, *43*, 719. (d) Reed, M. A. *Proc. IEE* **1999**, *87*, 652.
(4) Ziegler, C. In *Handbook of Organic Conductive Molecules and Polymers*; Nalwa, H. S., Eds.; Wiley: Chichester, U.K., 1997, Vol. 3, Chapter 13.
(5) Baüerle, P.; Fischer, T.; Bidlingmeier, B.; Stabel, A.; Rabe, J. P. *Angew. Chem., Int. Ed. Engl.* **1995**, *34*, 303.
(6) (a) Sirringhaus, H.; Brown, J. P.; Friend, R. H.; Nielsen, M. M.; Beechgard, K.; Langeveld-Voss, B. M. W.; Spiering, A. J. H.; Janssen, R. A. J.; Meijer, E. W.; Herwig, P.; de Leeuw, D. M. *Nature (London)* **1999**, *401*, 685. (b) Hoofman, R. J. O. M.; de Haas, M.; Siebbeles, L. D. A.; Warmann, J. M. *Nature (London)* **1998**, *392*, 54.
(7) Giesa, R. *J. Macromol. Sci. Rev. Chem. Phys.* **1996**, *C36*, 631.
(8) (a) Moroni, M.; Le Moigne, J.; Luzzati, S. *Macromolecules* **1994**, *27*, 562. (b) Wautelet, P.; Moroni, M.; Oswald, L.; Le Moigne, J.; Pham, A.; Bigot, J.-Y.; Luzzati, S. *Macromolecules* **1996**, *29*, 446.
(9) Tada, K.; Onoda, M.; Hirohata, M.; Kawai, T.; Yoshino, K. *Jpn. J. Appl. Phys.* **1996**, *35*, L251.
(10) Weder, C.; Wrighton, M. S. *Macromolecules* **1996**, *29*, 5157.
(11) Weder, C.; Sarwa, C.; Montali, A.; Bastiaansen, C.; Smith, P. *Science* **1998**, *279*, 835.
(12) Swager, T. M.; Gil, C. J.; Wrighton, M. S. *J. Phys. Chem.* **1995**, *99*, 4886.
(13) (a) Pschirer, N. G.; Miteva, T.; Evans, U.; Roberts, R. S.; Marshall, A. R.; Neher, D.; Myrick, M. L.; Bunz, U. H. F. *Chem. Mater.* **2001**, *13*, 2691. (b) Chu, Q.; Pang, Y.; Ding, L.; Karasz, F. E. *Macromolecules* **2002**, *35*, 7569.
(14) Kubel, C.; Mio, M. J.; Moore, J. S.; Martin, D. C. *J. Am. Chem. Soc.* **2002**, *124*, 8605.
(15) Levitsky, I. A.; Kim, J.; Swager, T. M. *J. Am. Chem. Soc.* **1999**, *121*, 1466.
(16) Breen, C. A.; Deng, T.; Breiner, T.; Thomas, E. L.; Swager, T. M. *J. Am. Chem. Soc.* **2003**, *125*, 9942.
(17) Levitus, M.; Schmieder, K.; Ricks, H.; Shimizu, K. D.; Bunz, U. H. F.; Garcia-Garibay, M. A. *J. Am. Chem. Soc.* **2001**, *123*, 4259.
(18) Kokil, A.; Shiyanovskaya, I.; Singer, K. D.; Weder, C. *J. Am. Chem. Soc.* **2002**, *124*, 9978.
(19) Giesa, R.; Schulz, R. C. *Makromol. Chem.* **1990**, *191*, 857.
(20) (a) Ballauff, M. *Makromol. Chem., Rapid Commun.* **1986**, *7*, 407. (b) Ballauff, M. *Makromol. Chem., Rapid Commun.* **1987**, *8*, 93. (c) Rodriquez-Prada, J. M.; Duran, R.; Wegner, G. *Macromolecules* **1989**, *22*, 2507.
(21) (a) Ofer, D.; Swager, T. M.; Wrighton, M. S. *Chem. Mater.* **1995**, *7*, 418. (b) C. Weder, M. S. Wrighton, *Macromolecules* **1996**, *29*, 5157.
(22) Skotheim, T. J., Ed.; *Handbook of Conducting Polymers*; Marcel Dekker: New York, 1986.
(23) (a) Schluter, A. D.; Rabe, J. P. *Angew. Chem., Int. Ed.* **2000**, *39*, 864. (b) Sheiko, S. S.; Moller, M. *Chem. Rev.* **2001**, *101*, 4099.
(24) (a) Mena-Osteritz, E.; Meyer, A.; Langeveld-Voss, B. M. W.; Janssen, R. A. J.; Meijer, E. W.; Bäuerle, P. *Angew. Chem., Int. Ed. Engl.* **2000**, *39*, 2680. (b) Grévin, B.; Rannou, P.; Payerne, R.; Pron, A.; Travers, J. P. *Adv. Mater.* **2003**, *15*, 881. (c) Lei, S. B.; Wan, L. J.; Wang, C.; Bai, C. L. *Adv. Mater.* **2004**, *16*, 828.
(25) (a) Lei, S. B.; Wang, C.; Yin, S. X.; Bai, C. L. *J. Phys. Chem. B* **2001**, *105*, 12272. (b) Qiu, X. H.; Wang, C.; Zeng, Q. D.; Xu, B.; Yin, S. X.; Wang, H. N.; Xu, S. D.; Bai, C. L. *J. Am. Chem. Soc.* **2000**, *122*, 5550. (c) Lu, J.; Lei, S. B.; Zeng, Q. D.; Kang, S. Z.; Wang, C.; Wan, L. J.; Bai, C. L. *J. Phys. Chem. B* **2004**, *108*, 5161.
(26) (a) De Feyter, S.; De Schryver, F. *Top. Curr. Chem.* **2005**, *258*, 205. (b) Cyr, D. M.; Venbataraman, B.; Flynn, G. W.; Black, A.; Whitesides, G. W. *J. Phys. Chem.* **1996**, *100*, 13747. (c) France, C. B.; Parkinson, B. A. *J. Am. Chem. Soc.* **2003**, *125*, 12712. (d) Giancarlo, L. C.; Flynn, G. *Acc. Chem. Res.* **2000**, *33*, 491.
(27) (a) Samorí, P.; Severin, N.; Müllen, K.; Rabe, J. P. *Adv. Mater.* **2000**, *12*, 579. (b) Samorí, P.; Francke, V.; Müllen, K.; Rabe, J. P. *Chem.—Eur. J.* **1999**, *5*, 2312.
(28) (a) Zhou, C. Z.; Liu, T. X.; Xu, J. M.; Chen, Z. K. *Macromolecules* **2003**, *36*, 1457. (b) Fan, Q. L.; Zhou, Y.; Lu, X. M.; Hou, X. Y.; Huang, W. *Macromolecules* **2005**, *38*, 2927.
(29) Becke, A. *J. Chem. Phys.* **1988**, *88*, 2547.
(30) Perdew, J. P.; Wang, Y. *Phys. Rev. B* **1992**, *45*, 13244.
(31) Bunz, U. H. F. *Chem. Rev.* **2000**, *100*, 1605.
(32) (a) Schumm, J. S.; Pearson, D. L.; Tour, J. M. *Angew. Chem.* **1994**, *33*, 1360. (b) Huang, S. L.; Tour, J. M. *J. Am. Chem. Soc.* **1999**, *121*, 4908. (c) Francke, V.; Mangel, T.; Müllen, K. *Macromolecules* **1998**, *31*, 2447.

MA062855N